# Flowing-afterglow study of electron-ion recombination of para–$H_3^+$ and ortho–$H_3^+$ ions at temperatures from 60 K to 300 K

Michal Hejduk,[1] Petr Dohnal,[1,a)] Peter Rubovič,[1] Ábel Kálosi,[1] Radek Plašil,[1] Rainer Johnsen,[2] and Juraj Glosík[1]
[1]*Department of Surface and Plasma Science, Faculty of Mathematics and Physics, Charles University in Prague, Prague 18000, Czech Republic*
[2]*Department of Physics and Astronomy, University of Pittsburgh, Pittsburgh, Pennsylvania 15260, USA*

(Received 9 April 2015; accepted 9 July 2015; published online 22 July 2015)

Detailed measurements employing a combination of a cryogenic flowing afterglow with Langmuir probe (Cryo-FALP II) and a stationary afterglow with near-infrared absorption spectroscopy (SA-CRDS) show that binary electron recombination of para–$H_3^+$ and ortho–$H_3^+$ ions occurs with significantly different rate coefficients, ${}^{p}\alpha_{bin}$ and ${}^{o}\alpha_{bin}$, especially at very low temperatures. The measurements cover temperatures from 60 K to 300 K. At the lowest temperature of 60 K, recombination of para–$H_3^+$ is at least three times faster than that of ortho–$H_3^+$ (${}^{p}\alpha_{bin} = (1.8 \pm 0.4) \times 10^{-7}$ cm$^3$ s$^{-1}$ *vs.* ${}^{o}\alpha_{bin} = (0^{+5}_{-0}) \times 10^{-8}$ cm$^3$ s$^{-1}$). © *2015 AIP Publishing LLC.* [http://dx.doi.org/10.1063/1.4927094]

## I. INTRODUCTION

$H_3^+$ ion is the most abundantly produced molecular ion in interstellar space[1] and plays a pivotal role in the reaction chains that form astrophysically important molecules like, e.g., $H_2O$ (Ref. 2) or simple hydrocarbons.[3] Dissociative recombination with electrons is one of the competing destruction mechanisms of $H_3^+$ ions in diffuse interstellar clouds[4] and, in part for this reason, has been studied experimentally and theoretically for more than 60 years.[5–7] Although much progress has been made in recent years, a true convergence between observational and laboratory data has not been achieved, and the situation is further complicated by the dependence of the recombination rate coefficient of $H_3^+$ ions on the nuclear spin configurations (para and ortho). Detailed discussions, preliminary conclusions, and comments on astrophysical relevance have been published (see, e.g., Ref. 8).

The present experiments focus on binary dissociative recombination of $H_3^+$ ions in specific nuclear spin states, namely,

$$ {}^{p}H_3^+ + e^- \xrightarrow{{}^{p}\alpha_{bin}} H_2 + H, H + H + H, \quad (1a) $$

$$ {}^{o}H_3^+ + e^- \xrightarrow{{}^{o}\alpha_{bin}} H_2 + H, H + H + H, \quad (1b) $$

where the "p" and "o" superscripts distinguish the para- and ortho-nuclear spin states of $H_3^+$. The corresponding binary recombination rate coefficients are denoted by ${}^{p}\alpha_{bin}$ and ${}^{o}\alpha_{bin}$. State-specific coefficients have been measured in storage-ring experiments by feeding para-enriched hydrogen to "cold" ion sources and varying the relative abundances of the two spin states of $H_3^+$.[9–16] Unfortunately, the results are now in doubt, as has been summarized, e.g., in Refs. 15, 17, and 18, because the abundances of the two spin states in the beam were not exactly known, and the rotational temperature of the ions was not as low as had been thought but was of the order or above 300 K.[15] The state-specific recombination of $H_3^+$ was studied also in afterglow experiments by monitoring the decay of a low temperature $H_3^+$ dominated afterglow plasma (predominantly in $He/Ar/H_2$ gas mixtures).[19–21] It is an advantage of the afterglow experiments that the abundances of para– and ortho–$H_3^+$ ions can be measured using absorption spectroscopy and that the ions are rotationally thermalized by multiple collisions with atoms/molecules of ambient neutral gas (see experimental confirmation and discussion in Refs. 19 and 22). Such afterglow experimental techniques (stationary afterglow (SA) and flowing afterglow with Langmuir probe (FALP)) are well established and relatively simple, have been extensively verified, but they are not entirely free of complications.[6,23,24] In our recent SA experiments, the density decays of $H_3^+$ ions in the particular spin state and their rotational thermalization within the para- and ortho-nuclear spin manifolds were monitored by near-infrared (NIR) Cavity Ring Down Spectroscopy (CRDS).[20,21,25]

One complication of afterglow experiments arises from additional ion loss processes (mainly ternary or third-body assisted recombination) that can contribute to the electron and ion density decays during the afterglow. It took over 50 years to realize that the discrepancies between rate coefficients measured in afterglow experiments were in part due to ternary neutral assisted recombination.[26] On the other hand, ternary processes involving neutrals or electrons (see, e.g., Refs. 27–31) are of interest for some applications and the plasma environment makes it possible to study them. For instance, our studies of recombination of $H_3^+$ ions in $He/Ar/H_2$ gas mixture showed that ternary He-assisted recombination of $H_3^+$ ions,

a)Petr.Dohnal@mff.cuni.cz

 

$$ {}^{p}H_3^+ + e^- + He \xrightarrow{{}^{p}K_{He}} \text{neutral products} + He, \quad (2a) $$

$$ {}^{o}H_3^+ + e^- + He \xrightarrow{{}^{o}K_{He}} \text{neutral products} + He, \quad (2b) $$

is a rather fast process.[19,20,26,30,32] Here, ${}^{p}K_{He}$ and ${}^{o}K_{He}$ are ternary recombination rate coefficients for pure para–$H_3^+$ and pure ortho–$H_3^+$. Recently, an even faster ternary $H_2$-assisted recombination of $H_3^+$ at 300 K was reported.[31] The theory of the ternary processes (2a) and (2b)[26,30,32] is not sufficiently developed to cleanly decompose experimental data into binary and ternary components. Hence, we are forced to measure recombination as a function of the third-body concentration (number of species in unit volume) and to obtain the binary recombination by extrapolating to zero third-body densities.

The state selective studies of $H_3^+$ recombination by Varju *et al.*[21] and Dohnal *et al.*[19,20] were limited to temperatures from 77 K to 200 K due to design limitations of the SA-CRDS apparatus. The measurements with SA-CRDS at 77 K showed that the binary recombination rate coefficient ${}^{p}\alpha_{bin}$ for para–$H_3^+$ is at 77 K at least three times higher than corresponding ${}^{o}\alpha_{bin}$ for ortho–$H_3^+$.[19] The ratio decreases with increasing temperature up to ≈200 K,[19] where both rate coefficients are comparable. The ternary recombination rate coefficients also showed small nuclear spin specificity at temperatures 140–200 K.[19]

The results of recent state selective afterglow (SA-CRDS) experiments[19–21] are in qualitative agreement with theoretical predictions.[33,34] However, at temperatures below ≈200 K, the difference between the coefficients ${}^{p}\alpha_{bin}$ and ${}^{o}\alpha_{bin}$ for the two nuclear spin manifolds seems to be increasing with decreasing temperature faster than predicted.[19,20,35] As mentioned earlier, storage-ring experiments have also produced state-selected cross sections at low collisional energies, but the rotational excitation of stored ions was of the order or above 300 K (see, e.g., discussion in Ref. 15 and in Reviews Refs. 17 and 18). Those experiments may eventually yield improved data but at this time, both the CRYRING (Electron Accelerator and Storage Ring Facility (Stockholm, Sweden))[10,13,16] and TSR (Test Storage Ring (Heidelberg, Germany))[9,11,15] facilities are closed and new cryogenic rings are being constructed.

Several authors have stated that the current state of knowledge on $H_3^+$ recombination is unsatisfactory and pointed out the need for further state-selective experimental studies at low temperatures with well-defined conditions and with several experimental techniques.[8,12] In astrochemistry, if para–$H_3^+$ really recombines faster than ortho–$H_3^+$ at temperatures below 200 K, the current models of rotational thermalization of $H_3^+$ ions and $H_2$ molecules in molecular clouds would have to be reformulated.[8,36] Astronomical observations of diffuse molecular clouds indicate that the population of fast recombining para–$H_3^+$ ions is higher than thermal.[37] This seriously questions generally accepted cosmic ray ionization rate of $H_2$ molecules.[8,38] Further experimental studies on nuclear spin specificity of rate coefficients of $H_3^+$ recombination with electron at temperatures below 200 K are needed and, if they confirm previous experimental results, they may require changes in the quantum-mechanical description of the recombination processes and a reevaluation of fundamental aspects of interstellar gas-phase chemistry.

This article contributes new experimental values of the state selected recombination rate coefficients ${}^{p}\alpha_{bin}$ and ${}^{o}\alpha_{bin}$ measured using our "Cryogenic Flowing Afterglow with Langmuir Probe" instrument (Cryo-FALP II) in the temperature range from 60 K to 210 K. In addition, we added new data to those of our previous SA-CRDS experiments in the temperature range from 80 K to 300 K. The two methods have different strengths and weaknesses: In the SA-CRDS afterglow, the electron and ion densities are sufficiently high ($\approx 3 \times 10^{10}$ cm$^{-3}$ at the onset of the afterglow phase) to infer recombination rates directly from *in situ* determinations of the density decays of para– and ortho–$H_3^+$ by optical absorption. In the Cryo-FALP II apparatus, the electron and ion densities are much lower ($\approx 5 \times 10^{8}$ cm$^{-3}$) and optical absorption measurements are not practical. Here, the recombination rates are inferred from the decay of the electron density measured by a Langmuir probe. In combined experiments, the relative concentrations of para– and ortho–$H_3^+$ ions are taken from the SA-CRDS data, measured at the same temperature and using the same hydrogen gas (either normal or para-enriched).

The higher electron densities in the SA-CRDS afterglow, however, can also enhance recombination by electron-assisted collisional radiative recombination (E–CRR), especially at very low temperatures because E–CRR depends very strongly on electron temperature (as $T_e^{-4.5}$). The SA-CRDS method is subject to a possible further problem: The discharge that produces the plasma can excite molecules (e.g., form vibrationally excited $H_2$). Some of them can survive into the afterglow phase and then transfer energy to the electron gas. In the Cryo-FALP II apparatus, the discharge region contains only helium and is well separated from the recombination region. These shortcomings of the SA-CRDS method were the main reasons why we decided to check and augment our earlier SA-CRDS measurements by similar measurements using Cryo-FALP II. As we will discuss later, the important conclusions remain the same as those reached earlier, namely, that at low temperatures, para–$H_3^+$ ions recombine with electrons much faster than ortho–$H_3^+$ ions.

In Sec. II, we will first describe the Cryo-FALP II apparatus, the para-hydrogen generator, and the SA-CRDS apparatus. After presenting results from SA-CRDS, we will discuss thermalization of $H_3^+$ ions in He/Ar/$H_2$ afterglow plasmas. The thermalization of electrons in the flowing afterglow plasma will be discussed in Sec. III. Determinations of state-specific recombination rate coefficients of $H_3^+$ ions will be discussed in Sec. IV. The temperature dependence of the recombination rate coefficients ${}^{p}\alpha_{bin}$ and ${}^{o}\alpha_{bin}$ of the state selected para–$H_3^+$ and ortho–$H_3^+$ will be presented in Sec. V.

## II. EXPERIMENTAL DETAILS

### A. Cryo-FALP II

The Cryo-FALP II (see Fig. 1) is a cryogenic high pressure modification of the FALP instrument,[6,39,40] whose technical details have been described earlier.[27,29,30,41] A movable cylindrical Langmuir probe (a 7 mm long tungsten wire, 18 μm in diameter) records the electron density[23,42,43] along the flow-tube axis (see Fig. 1). The three sections of the flow tube

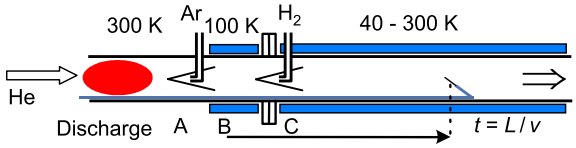


FIG. 1. The Cryo-FALP II apparatus (not to scale). The helium gas first passes through the microwave discharge. Ar and $H_2$ are added via two inlets located in the upstream part of sections B and C, respectively. The inner diameters of sections B and C are 5 cm. Section C, thermally insulated by a vacuum housing, is cooled by a closed-cycle helium refrigerator to adjustable temperatures down to 40 K. The electron density in section C is measured by the axially movable Langmuir probe.

(A–C) have different wall temperatures. Section A (made from Quartz) contains the microwave discharge and has a temperature of 300 K, section B is cooled to 100 K, while the temperature in the final section C can be varied from 40 K to 300 K, denoted as $T_{wall}$ in the following. The Langmuir probe can measure the electron density from the end of section B (position $L = 0$), passing through the connection of B and C (position $L = 5$ cm) and along section C.

A microwave discharge, ignited in helium buffer gas (with a number density $[He] \approx 10^{16}$–$10^{18}$ cm$^{-3}$) at the beginning of the section A of the flow tube, forms a plasma consisting of helium metastable atoms $He^m$, $He^+$, and $He_2^+$ ions. The plasma is carried by the helium flow downstream to section B where argon is added through an inlet (facing upstream to enhance gas mixing) at a density $[Ar] \approx 1.5 \times 10^{13}$ cm$^{-3}$ in order to convert the $He_2^+$ ions by charge transfer reactions to $Ar^+$ ions. The metastables $He^m$ are converted to $Ar^+$ ions by Penning ionization. This standard method has been described repeatedly (see, e.g., Ref. 23). Under the conditions of the experiment, the destruction of $He^m$ is essentially complete[39] in section B, even if the argon gas takes a finite time to blend into the helium flow (the so-called "end-effect"[44]).

The plasma then flows into section C of the flow tube that is cooled by a closed-cycle helium refrigerator to the desired temperature. At the beginning of section C (position $L = 5.5$ cm), either normal $H_2$ ($^nH_2$) or para-enriched $H_2$ ($^eH_2$) is introduced (at typical densities $[H_2] \approx 10^{12}$–$10^{13}$ cm$^{-3}$). The hydrogen mixes with the helium buffer gas and ion molecule reactions of $Ar^+$ ions with $H_2$ then form the recombining $H_3^+$ ions.[23,43] After the "transition region" (position $L = 5$ to 10 cm), the plasma becomes increasingly dominated by $H_3^+$ ions. In this region, the gas also cools down to $T_{wall}$ of section C. The thermalization of the gas can be observed by measuring the velocity of the gas (see Ref. 29). The measurements are carried out in the thermally equilibrated plasma.

We routinely employ a numerical model of the kinetic processes in the data analysis and to optimize conditions prior to every experiment (details can be found, e.g., in Refs. 23 and 31).

Our earlier studies[27–29] of E–CRR of $Ar^+$ ions proved that electrons and ions are in thermal equilibrium with the neutral gases in the recombination region and the same should be true in the present experiment. The hydrogen in the Cryo-FALP II experiment is never directly exposed to a microwave discharge and delayed heat sources, such as vibrationally excited hydrogen, are absent.

Rotational and vibrational modes of the formed $H_3^+$ ions are thermalized in subsequent collisions with He and $H_2$. This was shown in earlier SA-CRDS studies of the kinetic and rotational temperatures of $H_3^+$ ions under conditions similar to those in section C of the flow tube.[19,21,22]

### B. Para-hydrogen generator

We will denote the relative concentrations of para–$H_2$ hydrogen ($^pH_2$) and ortho–$H_2$ hydrogen ($^oH_2$) by $^pf_2$ and $^of_2$, respectively. In normal hydrogen ($^nH_2$) $^pf_2 = 0.25$ and $^of_2 = 0.75$. The symbol $^eH_2$ denotes para-enriched $H_2$ gas with $^pf_2 \approx 0.995$. The para-enriched hydrogen gas is produced using a "para-hydrogen generator" that converts $^oH_2$ to $^pH_2$ on a paramagnetic surface (thermally dehydrated $HFeO_2$, CAS number 20344–49–4), cooled down in a cryostat to temperatures 10–18 K.[45,46] In our experiment, $^nH_2$ is liquefied in the catalyst container and the saturated vapor of converted gas ($^eH_2$) is collected through an outlet tube that transfers it to the hydrogen ports of the Cryo-FALP II or the SA-CRDS. The flow of $^eH_2$ is controlled by varying the temperature of the catalyst container, i.e., by changing its vapor pressure. This configuration has been proved to provide a well-defined and constant value of $^pH_2$ equaling to (99.5 ± 0.5)%, which is the value obtained by measurement of the temperature dependence of the $N^+ + H_2$ reaction rate coefficient in an ion trap.[47] Only two flow-limiting valves are placed in the transfer tube to Cryo-FALP II or SA-CRDS to minimize para-to-ortho back conversion. If desired, the value of $^pf_2$ can be reduced by diluting $^eH_2$ with normal hydrogen $^nH_2$.[47]

### C. SA-CRDS. Measurements of kinetic and rotational temperatures and nuclear spin state of $H_3^+$ ions in the afterglow plasma

We denote the relative populations of para–$H_3^+$ ($^pH_3^+$) and ortho–$H_3^+$ ($^oH_3^+$) ions in an ensemble of $H_3^+$ ions by $^pf_3$ and $^of_3$ with $^pf_3 + {}^of_3 = 1$. Several studies of $^pf_3$ and $^of_3$ in low-temperature hydrogen plasmas have been conducted (see, e.g., Refs. 22, 48, and 49). In our recent SA-CRDS experiments, we systematically measured $^pf_3$ fractions during the active discharge and during the afterglow in He/Ar/$H_2$ mixtures similar to those used in the present work. We used $^nH_2$ or nearly pure $^pH_2$ and sometimes mixtures of $^nH_2$ and $^eH_2$ in order to obtain the desired value of $^pf_2$. The data measured during the recombination dominated afterglow in SA-CRDS experiments indicated that the values of $^pf_3$ are nearly independent on [He] and [$H_2$] in the density range covered by the experiments (see Figs. 3 and 4 in Ref. 50). The SA-CRDS experiments were carried out at temperatures 77–300 K. The absorption on two para-states and two ortho-states was used to monitor densities of para–$H_3^+$ and ortho–$H_3^+$ ions during the discharge and during the afterglow in SA-CRDS. The following second overtone transitions were used: $P(2,2) : 3v_2^1(1,2) \leftarrow 0v_2^0(2,2)$; $R(3,3)^l : 3v_2^1(4,3) \leftarrow 0v_2^0(3,3)$; $R(1,1)^u : 3v_2^1(2,1) \leftarrow 0v_2^0(1,1)$; $R(1,0) : 3v_2^1(2,0) \leftarrow 0v_2^0(1,0)$. The levels are labeled by their corresponding quantum numbers (J,G) (see Ref. 51). Further details of the CRDS technique used in recombination studies are given in Refs. 19, 21, 25, and 52.

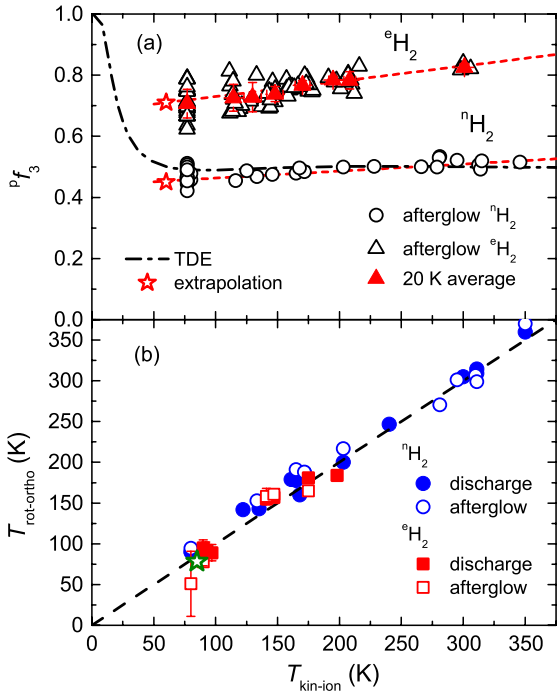


FIG. 2. SA-CRDS data. Panel (a) The temperature dependence of fraction $^{p}f_3$ of para–$H_3^+$ using either $^{n}H_2$ or $^{e}H_2$ as a precursor gas. Data were obtained during the early afterglow (empty symbols). To obtain average values, the temperature scale was divided into bins of length of 20 K and the values of $^{p}f_3$ measured in $^{e}H_2$ were averaged within each bin. The resulting 20 K averages are denoted by full triangles. The dashed-dotted line indicates $^{p}f_3$ calculated for thermodynamic equilibrium. Linear extrapolation of the $^{p}f_3$ data to 60 K along the dashed lines results in the values (star symbols) used in the analysis of Cryo-FALP II data at 60 K. Panel (b) The dependence of the rotational temperature $T_{rot\text{-}ortho}$ calculated from measured relative populations of $^{o}H_3^+$ (1,0) and $^{o}H_3^+$ (3,3) states of the $H_3^+$ ion on kinetic temperature of the ions $T_{kin\text{-}ion}$. New data were added to the previously measured values.[19] The green star denotes the rotational temperature $T_{rot\text{-}para}$ obtained from the measured populations of two para-states ($^{p}H_3^+$ (1,1) and $^{p}H_3^+$ (2,2)) in the afterglow plasma at 77 K in experiments with $^{e}H_2$. The dashed line indicates equality $T_{rot} = T_{kin\text{-}ion}$.

The CRDS absorption data yield the densities of ions in particular states, their kinetic and rotational temperatures and the dependence of the fractions $^{p}f_3$ on wall temperature $T_{wall}$ and the para-fraction of hydrogen $^{p}f_2$ (see panel (a) of Fig. 2). The kinetic temperature ($T_{kin\text{-}ion}$) of $H_3^+$ ions was determined from the Doppler broadening of the absorption lines. The conclusion from these studies is that in very good approximation $T_{kin\text{-}ion} = T_{wall}$, this implies also that $T_{wall} = T_{He}$. The present experiments with SA-CRDS confirm the results of earlier work (see, e.g., Fig. 1 in Ref. 21 and Figs. 5, 7, and 8 in Ref. 19) showing that $^{p}f_3$ is nearly time independent during the afterglow phase. Most importantly, it is evident that $^{p}f_3$ is enhanced when enriched hydrogen is the precursor gas[22] and that $^{p}f_3$ depends only weakly on temperature in the range from 77 K to 300 K. Examples of data measured during the afterglow in experiments with $^{n}H_2$ or $^{e}H_2$ as a precursor gas are shown in panel (a) of Fig. 2. In the present study, we also confirmed previous result that the values of $^{p}f_3$ measured during the discharge and during the afterglow are nearly the same.

The rotational temperature $T_{rot\text{-}ortho}$ was determined by measuring densities of ions in two rotational states of the ortho manifold. In some experiments, the discharge tube was immersed in liquid nitrogen ($T_{wall}$ = 77 K) and the rotational temperature for the para-manifold $T_{rot\text{-}para}$ was also determined. The dependence of the measured $T_{rot}$ on the measured $T_{kin\text{-}ion}$ is plotted in panel (b) of Fig. 2. It is obvious that the two temperatures are essentially the same.

From the experiments with SA-CRDS, we concluded that the $H_3^+$ ions in the afterglow plasma are very close to thermal equilibrium with the helium buffer gas, which in turn is in good thermal contact with the wall of the discharge tube. Hence, we are justified in assuming that $T = T_{wall} = T_{He} = T_{rot} = T_{kin\text{-}ion}$. Because of the relatively high He density and very low microwave power used for plasma generation, the same assumption can be made for the plasma in the discharge just before termination of the microwave pulse. The experimental data confirm this conclusion (see Fig. 2). Although this is not crucial for the recombination measurements, we note that the ion temperature varies slowly during the transition from the active discharge to the afterglow. In contrast, the electron temperature changes rather abruptly.

An experimental verification of the thermal equilibrium assumption is essential in the analysis of the SA-CRDS measurements because otherwise total ion densities and electron densities in SA-CRDS could not be inferred from the measured absorption strengths of particular transitions. Also, the separation of the measured effective recombination coefficient into the components due to para–$H_3^+$ and ortho–$H_3^+$ is possible only if the relative fractions of the two species remain constant during the afterglow, even if one species recombines faster than the other.

## III. ELECTRON TEMPERATURE IN HE/AR/$H_2$ AFTERGLOW PLASMA IN CRYO-FALP II

The electron temperature, $T_e$, is a key plasma parameter but there is no simple direct way of measuring it with good accuracy at low temperatures. Measurements of ambipolar diffusion losses in the late afterglow provide a reasonably accurate "proxy thermometer." The reciprocal time constant describing the ambipolar diffusion loss in a container with fundamental diffusion length Λ can be derived from the basic relations contained in the book of Mason and McDaniel[53] as

$$\frac{1}{\tau_D} = 4.63 \times 10^{15} \frac{K_0(T)}{\Lambda^2} \frac{T}{[\mathrm{He}]}\ \mathrm{s}^{-1}, \qquad (3)$$

where $K_0(T)$ is the reduced mobility of the ion (in units $cm^2\ V^{-1}\ s^{-1}$), the fundamental diffusion length Λ is in cm, temperature $T$ in K, and helium number density [He] in $cm^{-3}$. For cylindrical geometry, the value of Λ can be calculated[53] as $1/\Lambda^2 = (J_0/r)^2 + (\pi/l)^2$, where $J_0$ is the first root of the zeroth order Bessel function, $J_0 \approx 2.405$, $r$ is the radius of the flow tube, and $l$ is the length of the flow tube. In our case, $r$ = 2.5 cm, $l \approx 60$ cm, and $\Lambda^2 = 1.1\ cm^2$. If measurements of $\tau_D$ in the late afterglow (after recombination becomes negligible) agree with this formula, then one can conclude that the electron and neutral temperatures are nearly equal.

We have used the same method successfully in our Cryo-FALP II measurements of E–CRR and helium-assisted collisional radiative recombination (He–CRR) of $Ar^+$ ions.[27–29] The

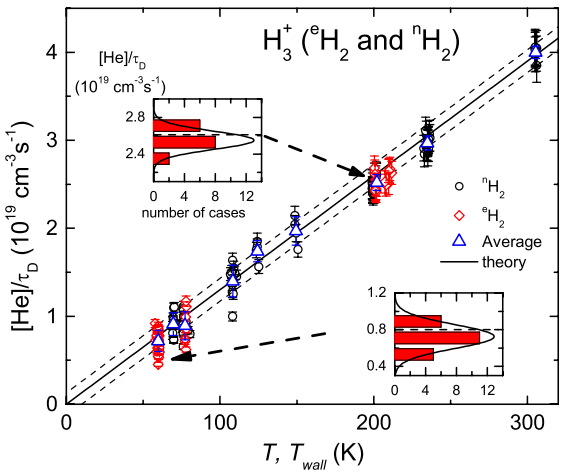


FIG. 3. Cryo-FALP II data. The measured reciprocal time constant of ambipolar diffusion losses $[\mathrm{He}]/\tau_D$ as a function of the wall temperature ($T_{wall}$). Circle and diamond symbols: data obtained using $^nH_2$ or $^eH_2$, respectively. Triangles: average values at a particular temperature. Solid line: values calculated from Eq. (3) as a function of the temperature $T = T_{wall}$. Dashed lines: the same as the solid line but calculated for alternate temperatures $T_e = T_{wall} \pm 20$ K. Insets: frequency distribution of the data at $T_{wall} = 60$ K and $T_{wall} = (204 \pm 3)$ K, fitted to a normal distribution. The width of each bin is $1.8 \times 10^{18}$ cm$^{-3}$ s$^{-1}$. The dashed lines refer to the calculated value of $[\mathrm{He}]/\tau_D$ at a given temperature.

ternary rate coefficients of both processes depend very strongly on electron temperature ($K_{\mathrm{E–CRR}} \propto T_e^{-4.5}$, $K_{\mathrm{He–CRR}} \propto T_e^{-2.5}$) so that measurements of their values provide a sensitive test of the electron-temperature scale.[19,27–29,54] It was found that the electron temperature was always close to the gas temperature within a few kelvins.

The same type of measurement of diffusion losses in $H_3^+$ afterglows using Cryo-FALP II yielded the graph in Fig. 3. The data follow the calculated line very well, but the data scatter at the lowest temperatures and high helium densities is noticeably worse. This is a consequence of the fact that the diffusion rate becomes very small and that recombination in the late afterglow is not entirely negligible. The full line is calculated using a zero-field reduced mobility of $K_0(300\ \mathrm{K}) = 30.5\ \mathrm{cm^2\ V^{-1}\ s^{-1}}$, adopted from Ref. 55. To show the sensitivity to small deviations in temperature, we also calculated alternate values of $[\mathrm{He}]/\tau_D$ for $T_e \pm 20$ K (the dashed lines). There was no detectable difference between experiments with $^nH_2$ and $^eH_2$ that are distinguished by different symbols, circles, and diamonds.

The data presented in Figs. 2 and 3 support the assumption that the various temperatures in the Cryo-FALP II afterglow have a common value, i.e., that $T = T_{wall} = T_{He} = T_{rot} = T_{kin\text{-}ion} = T_e$. The rotational states are in equilibrium within the para–$H_3^+$ or the ortho–$H_3^+$ nuclear spin manifolds, but because of nuclear spin restrictions in the reactions of $^{p/o}H_2$ with $^{p/o}H_3^+$, the fraction $^pf_3$ also depends on the $^pf_2$ value of the used hydrogen gas. The value of $^pf_3$ corresponds to the thermodynamic equilibrium (TDE) only for experiments with $^nH_2$ and only at temperatures above ≈77 K (see panel (a) of Fig. 2 and also Figs. 7 and 8 in Ref. 22). We stress that our experimental verification that $T_e = T_{He}$ is important. One could reach the same conclusion by considering only elastic energy transfer between electrons and helium atoms, which is quite efficient at the experimental helium densities, but this leaves out possible electron heating by superelastic collisions with remaining metastable helium atoms and excited argon atoms. Such heat sources do not seem to play a role in the Cryo-FALP II experiments, as we had concluded earlier from our experiments on E–CRR and He–CRR.[27–29] We should also note, however, that the same may not be true in SA-CRDS measurements (see also the discussion in Sec. V B).

## IV. DETERMINATION OF STATE-SPECIFIC RECOMBINATION RATE COEFFICIENTS

The methods of obtaining state-specific recombination rate coefficients are essentially identical in the Cryo-FALP II and in the SA-CRDS studies.[19–21] In the Cryo-FALP II experiment, we measure the decay of the electron number density $n_e$ by the Langmuir probe but the values of $^pf_3 = {}^pf_3(^pf_2, T)$ are taken from the SA-CRDS studies. The effective recombination rate coefficient $\alpha_{eff}$ is defined by the relation,

$$\frac{\mathrm{d}n_e}{\mathrm{d}t} = -\alpha_{eff}\, n_e^2 - \frac{n_e}{\tau_D}, \tag{4}$$

where $\tau_D$ is the characteristic time of ambipolar diffusion. As usual, it is assumed that the afterglow plasma is quasineutral. The measured value of $\alpha_{eff}$ is a weighted sum of the effective recombination rate coefficients of $^pH_3^+$ and $^oH_3^+$ ions, i.e.,

$$\alpha_{eff} = {}^pf_3\, {}^p\alpha_{eff} + {}^of_3\, {}^o\alpha_{eff}, \tag{5}$$

where $^p\alpha_{eff}$ and $^o\alpha_{eff}$ are the effective recombination rate coefficients of pure $^pH_3^+$ and pure $^oH_3^+$, respectively. Both $^p\alpha_{eff}$ and $^o\alpha_{eff}$ can then be obtained from measurements of $\alpha_{eff}$ ($H_3^+$) for two or more different values of $^pf_3$. These values are still "effective" values and are not necessarily equal to the corresponding binary recombination coefficients.

Examples of the electron-density decays measured in experiments at $T = 60$ K with $^eH_2$ and $^nH_2$ are shown in Figure 4. The electron densities are plotted as functions of the Langmuir probe position $L$ and the equivalent afterglow time $t = v/L$, where $v$ is the plasma flow velocity.[29] All recombination measurements are carried out in the thermally equilibrated plasma where $H_3^+$ decays mainly by recombination and diffusion to the walls, as is assumed in Eq. (4). Panel (a) of Figure 4 only shows the time evolutions of electron densities in this region. Note that losses due to recombination and due to diffusion are comparable.

The desired binary recombination coefficients are obtained by extrapolating values of $\alpha_{eff}$ measured at different hydrogen and helium densities to zero densities. We have suggested possible mechanisms leading to density dependences earlier (see Refs. 26 and 31) but this is not essential for the present work and we omit the details. Fig. 5 shows an example of the dependence of $\alpha_{eff}$ (observed at 60 K) on hydrogen density at different fixed helium densities, while Fig. 6 shows the dependence of $\alpha_{eff}$ on helium density for fixed hydrogen densities. Linear extrapolations to zero densities of He and $H_2$ yield binary recombination coefficients at 60 K that are larger when enriched hydrogen is substituted for normal hydrogen. The data sets measured in Cryo-FALP II at higher

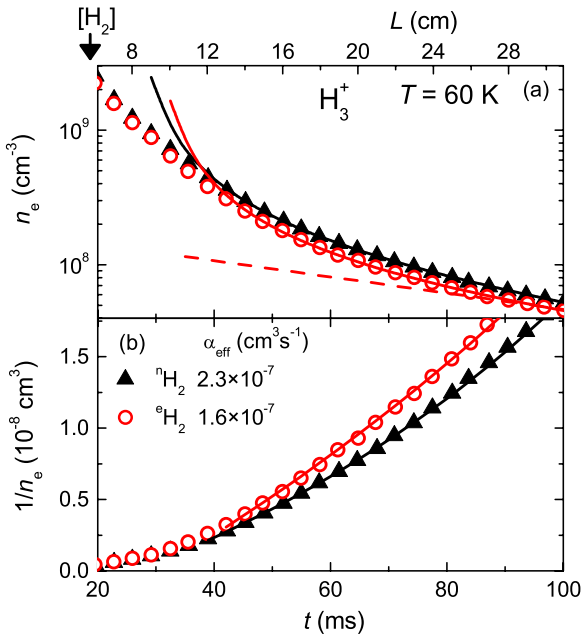


FIG. 4. Cryo-FALP II data. Panel (a) Examples of electron density $n_e$ decays, as measured by the movable Langmuir probe, observed when $H_3^+$ ions are formed by reactions with either normal ($^nH_2$, triangles) or para-enriched hydrogen ($^eH_2$, circles). Time ($t$, lower axis) and position ($L$, upper axis) are related by the helium flow velocity.[29] The arrow indicates the position of the hydrogen entry port at the beginning of the section C of the flow tube (see Fig. 1). The full lines are fits to the data (for details on data analysis, see Ref. 42). The dashed line indicates the decay due to ambipolar diffusion losses for the experiment with $^eH_2$. Panel (b) The time evolutions of the reciprocal electron number density ($1/n_e$). The data were obtained at $T = 60$ K, $P_{He} = 480$ Pa, [Ar] = $1.6\times10^{13}$ cm$^{-3}$, [$^nH_2$] = $1.5\times10^{12}$ cm$^{-3}$, [$^eH_2$] = $1.0\times10^{12}$ cm$^{-3}$.

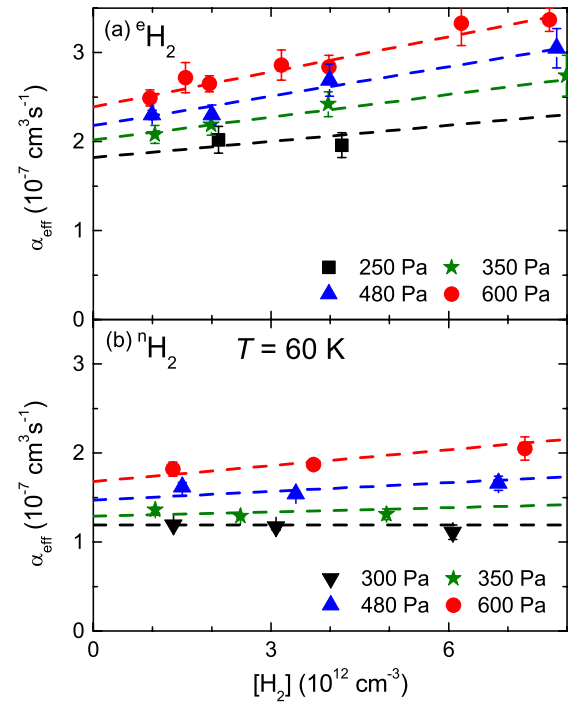


FIG. 5. Cryo-FALP II data. Dependence of $\alpha_{eff}$ on $H_2$ density measured at 60 K at the indicated pressures of helium. Panels (a) and (b) show data measured in the experiments with $^eH_2$ and $^nH_2$, respectively.

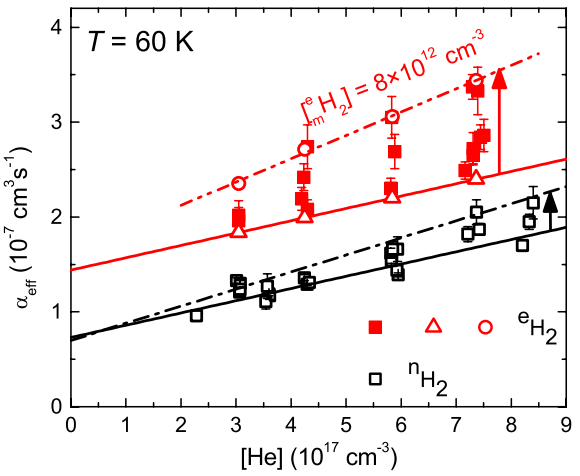


FIG. 6. Cryo-FALP II data. Dependence of $\alpha_{eff}$ at $T = 60$ K on helium density in experiments with $^eH_2$ (full squares) and with $^nH_2$ (open squares). The arrows indicate the increase of $\alpha_{eff}$ with increasing density of $H_2$ at fixed [He]. Open triangles and open circles indicate values obtained at the limits for [$^eH_2$] → 0 and [$^eH_2$] → $8\times10^{12}$ cm$^{-3}$, respectively. The solid lines are linear fits of the data measured at low hydrogen densities. Dashed-dotted-dotted and dashed-dotted lines are fits of the data at high hydrogen density, in the experiment with $^eH_2$ and $^nH_2$, respectively.

temperatures (78 K and 210 K) are similar to the 60 K data but the difference between data with normal and enriched hydrogen becomes smaller as $T$ increases.

The dependence of $\alpha_{eff}$ on [He] and on [$H_2$] shown in Figs. 5 and 6 is actually somewhat more complex than it appears in Figs. 5 and 6. To illustrate this, we also plotted the same data in the form of a 3-dimensional graph, shown in Fig. 7. The data are fitted by the equation

$$^{e/n}\alpha_{eff} = {}^{e/n}\alpha_{bin} + {}^{e/n}\xi_1[He] + {}^{e/n}\xi_2[H_2] + {}^{e/n}\xi_3[He][H_2], \quad (6)$$

where $^{e/n}\xi_1$, $^{e/n}\xi_2$, and $^{e/n}\xi_3$ are constants at a given temperature. The superscripts refer to the type of hydrogen used in the

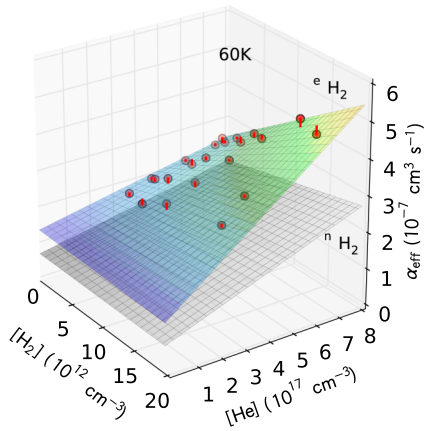


FIG. 7. Cryo-FALP II data. Dependence of $^e\alpha_{eff}$ and $^n\alpha_{eff}$ on [He] and [$H_2$] measured at $T = 60$ K in experiments with $^eH_2$ and with $^nH_2$, respectively. The upper surface is a fit of Eq. (6) to the data (indicated by circles) obtained with $^eH_2$. The lower surface represents a fit of Eq. (6) to the data obtained with $^nH_2$ (data points are omitted for clarity). The data points deviate from the surfaces by amounts on the order $<2\times10^{-8}$ cm$^3$ s$^{-1}$ as is shown by red lines connecting the data points with the plane. The parameters of the fits are listed in Table I.

TABLE I. The fitting parameters $\xi_1$, $\xi_2$, and $\xi_3$ for the data obtained at $T = 60$ K in experiments with $^{n}H_2$ and $^{e}H_2$ hydrogen (see Figure 7). Values $\xi_1$, $\xi_2$, and $\xi_3$ are given in format $\xi_{i0}(m)$ indicating $\xi_i = \xi_{i0} \times 10^m$. For comparison, the values $^{e/n}\alpha_{bin}$ and contributions from $\xi_1$[He], $\xi_2[H_2]$, and $\xi_3[H_2]$[He] terms are given in units $10^{-7}$ cm$^3$ s$^{-1}$. The values are deduced from Equation (6) using fitting parameters $\xi_1$, $\xi_2$, $\xi_3$ for typical densities of $H_2$ and He, [He] = $5 \times 10^{17}$ cm$^{-3}$, [$H_2$] = $5 \times 10^{12}$ cm$^{-3}$.

| 60 K gas | $^{e/n}\alpha_{bin}$ ($10^{-7}$ cm$^3$ s$^{-1}$) | $\xi_1$[He] ($10^{-7}$ cm$^3$ s$^{-1}$) | $\xi_2[H_2]$ ($10^{-7}$ cm$^3$ s$^{-1}$) | $\xi_3[H_2]$[He] ($10^{-7}$ cm$^3$ s$^{-1}$) | $\xi_1$ (cm$^6$ s$^{-1}$) | $\xi_2$ (cm$^6$ s$^{-1}$) | $\xi_3$ (cm$^9$ s$^{-1}$) |
|---|---|---|---|---|---|---|---|
| $^{n}H_2$ | 0.75 | 0.65 | 7.0(−12) | 0.15 | 1.29(−25) | 1.4(−31) | 5.8(−39) |
| $^{e}H_2$ | 1.44 | 0.66 | −1.5(−12) | 0.45 | 1.32(−25) | −3.0(−32) | 1.8(−38) |

experiment. The binary values $^{e}\alpha_{bin}$ and $^{n}\alpha_{bin}$ are those in the limits [He] → 0 and [$H_2$] → 0.

The fitting parameters for the data measured at 60 K with $^{n}H_2$ and $^{e}H_2$ are given in Table I. Listed are also the contributions from all four terms of function (6) deduced for typical densities of $H_2$ and He in experiments ([He] = $5 \times 10^{17}$ cm$^{-3}$, [$H_2$] = $5 \times 10^{12}$ cm$^{-3}$). The contributions from the third term $\xi_2[H_2]$ are very low in comparison with contributions from other terms. The contribution from $\xi_3[H_2]$[He] is comparable with $^{e/n}\alpha_{bin}$ and with contribution from $\xi_1$[He], and hence, the best-fitting surfaces are not planes but are slightly twisted. More twisted is the surface obtained from data measured with $^{e}H_2$. This may indicate the existence of a loss process that depends on the product [He][$H_2$] and this process is more effective for $^{e}H_2$ (see also Fig. 6). It is possible that part of the observed recombination loss is due to $H_5^+$ ions that are formed by three-body association involving both helium and hydrogen, but the data do not allow a firm conclusion. The inference of the binary recombination rates is not affected by this ambiguity.

## V. RESULTS AND DISCUSSION

### A. Temperature dependence of the rate coefficients

Sections III and IV point out the experimental difficulties in measuring state specific binary recombination coefficients for $H_3^+$ in the two nuclear spin states. One needs large data sets at different gas densities and has little choice but to obtain the final result by extrapolation. In this section, we show that the results obtained by different methods are nevertheless quite consistent.

The results of the Cryo-FALP II measurements of $^{p}\alpha_{bin}$ and $^{o}\alpha_{bin}$ at different temperatures (60 K, 78 K, and 210 K) are compared to those obtained in the parallel SA-CRDS experiment in Fig. 8. The graph includes new SA-CRDS data of $^{n}\alpha_{eff}$ and $^{e}\alpha_{eff}$ at 115 K, 145 K, 180 K, and 300 K obtained by *in situ* determination of $^{p}f_3$ and data obtained in our earlier SA-CRDS experiments[19–21,50] at temperatures 85 K, 140 K, 165 K, and 195 K. In addition, the graph shows values of $^{n}\alpha_{eff}$ measured in FALP, SA-CRDS, and Cryo-FALP II experiments with $^{n}H_2$ as precursor gas to form $H_3^+$ ions (see Ref. 41).

The rate coefficients $^{p}\alpha_{bin}$ and $^{o}\alpha_{bin}$ obtained in the Cryo-FALP II experiments are in good agreement with the values obtained in SA-CRDS experiments in the covered temperature range. In our previous studies, we also observed agreement between values of $^{n}\alpha_{bin}$ measured by SA-CRDS and by FALP/Cryo-FALP II (see Ref. 41). This is particularly noteworthy because these two experiments differ greatly in the formation of the $H_3^+$ plasma, in the electron/ion densities, in the time scale of the plasma decay, and in the diagnostics used to determine the parameters of the afterglow plasma. Within the accuracy of the experimental data, there is also good agreement with the storage ring data at 300 K[9,16] that are indicated by arrows on the right hand side of the graph. The values of $^{p}\alpha_{bin}$, $^{o}\alpha_{bin}$, and $^{n}\alpha_{bin}$ are given in the summarization of CRYRING data for 300 K in Ref. 13. At lower temperatures, there are no accurate data from storage rings to compare.[15] Figure 8 also shows the theoretical temperature dependences of the binary recombination rate coefficients for pure para–$H_3^+$, pure

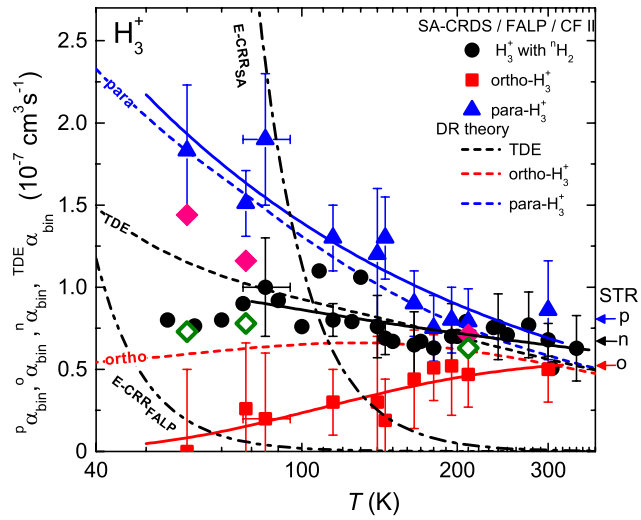


FIG. 8. Cryo-FALP II and SA-CRDS. Nuclear spin state-specific binary recombination rate coefficients measured in Cryo-FALP II, FALP, and SA-CRDS experiments. Triangles and squares indicate $^{p}\alpha_{bin}$ and $^{o}\alpha_{bin}$, respectively. The values at 85 K, 140 K, 165 K, and 195 K were taken from our previous experiments.[19] The values of $^{n}\alpha_{bin}$ (circles) were measured in the Cryo-FALP II, FALP, and SA-CRDS experiments and some data were taken from our previous studies.[19,41] The diamonds refer to $^{n}\alpha_{bin}$ (open diamonds) and $^{e}\alpha_{bin}$ (closed diamonds) measured in the present Cryo-FALP II experiment. The full lines are fits to $^{p}\alpha_{bin}$, $^{o}\alpha_{bin}$, and $^{n}\alpha_{bin}$ to the function in Eq. (7) that is used in astrophysical databases. For details and for the parameters of the fits see the text and Table II. The arrows on the right hand side of the figure denoted as p, o, and n indicate the values of $^{p}\alpha_{bin}$, $^{o}\alpha_{bin}$, and $^{n}\alpha_{bin}$ obtained in CRYRING,[13] respectively. The dashed lines indicated as para, ortho, and thermodynamic equilibrium (TDE) are theoretical dependences for para–$H_3^+$, ortho–$H_3^+$, and for $H_3^+$ ions in TDE.[33,35] The dashed-dotted lines E–$CRR_{SA}$ and E–$CRR_{FALP}$ are effective binary rate coefficients of ternary E–CRR calculated for electron number densities $n_e$(SA-CRDS) = $3 \times 10^{10}$ cm$^{-3}$ and $n_e$(Cryo-FALP II) = $5 \times 10^8$ cm$^{-3}$.[19,27–29]

TABLE II. Parameters $\alpha_{\text{A-K}}$, $\beta$, and $\gamma$ of the fit by Arrhenius-Kooij formula (7). The values of ${}^{\text{p}}\alpha_{\text{bin}}$ and ${}^{\text{o}}\alpha_{\text{bin}}$ plotted in Fig. 8 were fitted for 60–300 K. The values of ${}^{\text{n}}\alpha_{\text{bin}}$ were fitted for 77–340 K. As it is discussed above (see Fig. 2), in this temperature range, the afterglow plasma with ${}^{\text{n}}H_2$ is in thermal equilibrium including the para to ortho $H_3^+$ ratio. The values of ${}^{\text{p}}\alpha_{\text{bin}}$ (300 K), ${}^{\text{o}}\alpha_{\text{bin}}$ (300 K), and ${}^{\text{TDE}}\alpha_{\text{bin}}$ (300 K) were measured in SA-CRDS experiment. The values of ${}^{\text{p}}\alpha_{\text{bin}}$ (60 K) and ${}^{\text{o}}\alpha_{\text{bin}}$ (60 K) for para–$H_3^+$ and ortho–$H_3^+$ were obtained from data measured in the Cryo-FALP II experiment. The value ${}^{\text{TDE}}\alpha_{\text{bin}}$ (60 K) for $H_3^+$ in TDE is calculated from the measured ${}^{\text{p}}\alpha_{\text{bin}}$ and ${}^{\text{o}}\alpha_{\text{bin}}$ and from ${}^{\text{p}}f_3$ calculated for $H_3^+$ in TDE at $T = 60$ K.

| Ion | ${}^{\text{p/o/TDE}}\alpha_{\text{bin}}$ (60 K) ($10^{-7}$ cm$^3$ s$^{-1}$) | ${}^{\text{p/o/TDE}}\alpha_{\text{bin}}$ (300 K) ($10^{-7}$ cm$^3$ s$^{-1}$) | $\alpha_{\text{A-K}}$ ($10^{-7}$ cm$^3$ s$^{-1}$) | $\beta$ | $\gamma$ (K) |
|---|---|---|---|---|---|
| Para–$H_3^+$ | (1.8 ± 0.4) | (0.86 ± 0.30) | (0.69 ± 0.08) | (−0.64 ± 0.10) | 0 |
| Ortho–$H_3^+$ | $(0.0^{+0.5}_{-0.0})$ | (0.50 ± 0.20) | (0.97 ± 0.40) | (−0.41 ± 0.91) | (187 ± 143) |
| $H_3^+$ (TDE) | $(0.9^{+0.6}_{-0.4})$ | (0.68 ± 0.10) | (0.65 ± 0.04) | (−0.26 ± 0.07) | 0 |

ortho–$H_3^+$, and for $H_3^+$ ions in TDE.[33,35] The theoretical results of ${}^{\text{TDE}}\alpha_{\text{bin}}$ by Ch. Jungen and S. T. Pratt[34] are nearly identical and are not shown.

For compatibility of our results with databases used in astrophysics, the measured recombination rate coefficients are fitted by the Arrhenius-Kooij formula as used in the KIDA database,[56]

$$k_{\text{Kooij}}(T) = \alpha_{\text{A-K}}(T/300\ \text{K})^{\beta} \exp(-\gamma/T), \tag{7}$$

where $\alpha_{\text{A-K}}$, $\beta$, and $\gamma$ are free parameters. The values $k_{\text{Kooij}}$ and $\alpha_{\text{A-K}}$ are in cm$^3$ s$^{-1}$, $\beta$ is dimensionless, the temperature and the parameter $\gamma$ are in K. The parameters of the fit of the values of ${}^{\text{p}}\alpha_{\text{bin}}$ and ${}^{\text{o}}\alpha_{\text{bin}}$ for temperatures 60–300 K and of the values of ${}^{\text{n}}\alpha_{\text{bin}}$ for 77–340 K are given in Table II. Together with actual values of ${}^{\text{n}}\alpha_{\text{bin}}$ ${}^{\text{p}}\alpha_{\text{bin}}$, and ${}^{\text{o}}\alpha_{\text{bin}}$ measured at 60 K and 300 K. Note that parameters $\alpha_{\text{A-K}}$, $\beta$, and $\gamma$ are different for para–$H_3^+$, ortho–$H_3^+$, and $H_3^+$ in TDE. The corresponding values of $k_{\text{Kooij}}(T)$ calculated from Eq. (7) are plotted in Fig. 8 as full lines.

### B. Possible contribution of E–CRR in recombination of $H_3^+$

It is well known that recombination in low-temperature plasmas can also occur by E–CRR that proceeds by three-body electron capture into high Rydberg states and subsequent cascading to lower Rydberg states. The effective (apparent) binary rate coefficients, $\alpha_{\text{E–CRR}} \sim 3.8 \times 10^{-9}\ n_e T_e^{-4.5}$ cm$^3$ s$^{-1}$,[27–29,54] are indicated by the dashed-dotted lines in Fig. 8 for typical electron densities in the SA-CRDS ($n_e$(SA-CRDS) = $3 \times 10^{10}$ cm$^{-3}$) and in the Cryo-FALP II ($n_e$(Cryo-FALP II) = $5 \times 10^8$ cm$^{-3}$) experiments. At the higher electron densities in the SA-CRDS experiment, the effective binary E–CRR recombination rate coefficient actually becomes larger than our measured values at temperatures below $T \approx 100$ K, which is peculiar and rather disturbing. In the Cryo-FALP II experiment, the electron densities are smaller by a factor of 60 and E–CRR should be nearly negligible. Both experiments, however, give almost the same values for the $H_3^+$ recombination rate coefficients. One, however unlikely, explanation might be that the formula for the E–CRR recombination is not valid at low temperatures. This explanation was ruled out by our recent experiments on E–CRR of atomic $Ar^+$ ions using Cryo-FALP II[28,29] which confirmed the standard E–CRR formula at low temperatures down to 50 K. These experiments leave open the possibility that E–CRR of a molecular ion, such as $H_3^+$, is much slower than that of atomic ions. To the best of our knowledge, there are no pertinent experiments or theories that support or refute such an *ad hoc* assumption. It is also possible and perhaps more likely that the electron temperatures in the SA-CRDS experiments were higher than the gas temperatures and that E–CRR was hence strongly reduced. In the Cryo-FALP II experiments, E–CRR should be absent and this was one reason why we performed them. We conclude that the main result of the present study is not affected by E–CRR and that ${}^{\text{p}}\alpha_{\text{bin}}$ is much larger than ${}^{\text{o}}\alpha_{\text{bin}}$.

### C. Sources of errors

The random errors in the effective recombination rate coefficients measured in SA-CRDS and Cryo-FALP II experiments are less than 5%. In the Cryo-FALP II experiment, the main systematic errors arise from the evaluation of the electron number density by the Langmuir probe that is calibrated by measurements of a well-known rate coefficient of $O_2^+$ recombination.[27] The estimated uncertainty of recombination rate coefficients measured in Cryo-FALP II experiment is 20%. A systematic error of the SA-CRDS experiment arises from the uncertainty of the length of the plasma column and is on the order of 10%. The state specific recombination rate coefficients measured in the Cryo-FALP II experiment are also subject to errors originating from the uncertainty of ${}^{\text{p}}f_3$ which we estimated at 5% (in SA-CRDS experiment, the value of ${}^{\text{p}}f_3$ is measured directly).

## VI. CONCLUSION

We measured nuclear spin state-specific $H_3^+$ recombination rate coefficients ${}^{\text{p}}\alpha_{\text{bin}}$ and ${}^{\text{o}}\alpha_{\text{bin}}$ for para–$H_3^+$ and ortho–$H_3^+$ in the temperature range 60–300 K employing Cryo-FALP II and SA-CRDS experiments. This is the first time that state selected recombination rate coefficients have been measured down to 60 K using a FALP type experiment with variable relative population of para–$H_3^+$ and ortho–$H_3^+$. It is gratifying to note that results obtained by two distinct experiments and a combination of them are mutually consistent. As the temperature decreases, the difference between binary ${}^{\text{p}}\alpha_{\text{bin}}$ and

$^{o}\alpha_{bin}$ increases: at 60 K, para–$H_3^+$ recombines with an at least a factor of three higher rate coefficient than ortho–$H_3^+$, $^{p}\alpha_{bin}(60\ K) = (1.8 \pm 0.4) \times 10^{-7}\ cm^3\ s^{-1}$ *vs.* $^{o}\alpha_{bin}(60\ K) = (0^{+5}_{-0}) \times 10^{-8}\ cm^3\ s^{-1}$. The measured temperature dependence of $^{TDE}\alpha_{bin}$ for ions in TDE and $^{p}\alpha_{bin}$ and $^{o}\alpha_{bin}$ for pure para–$H_3^+$ and ortho–$H_3^+$ agrees well with modern theories.[33–35] The existence of two groups of $H_3^+$ ions with very different recombination rate coefficients at low temperatures should be seriously considered in astrochemical models of the interstellar medium. The results presented here depend on an assumption that there are no unrecognized strong pressure dependences below the lowest experimental pressures. The seeming absence of E-CRR of $H_3^+$ ions in SA-CRDS experiment is also disturbing. Further experiments performed in an environment of lower pressures with negligible influence of three body effects (such as in the merged beams technique), under good control of the $H_3^+$ rotational temperature and ortho/para-populations, remain desirable as a verification in the future.

## ACKNOWLEDGMENTS

This work was partly supported by Czech Science Foundation Project Nos. GACR P209/12/0233, GACR 14-14649P, and GACR 15-15077S and by Charles University in Prague Project Nos. GAUK 659112, GAUK 692214, GAUK 572214, UNCE 204020/2012, and SVV 260 090.

[1]T. Oka, Proc. Natl. Acad. Sci. U. S. A. **103**, 12235 (2006).
[2]A. Dalgarno, in *Advances in Atomic, Molecular, and Optical Physics*, edited by B. Bederson and A. Dalgarno (Academic Press, 1994), Vol. 32, pp. 57–68.
[3]J. Tennyson, in *Handbook of Molecular Physics and Quantum Chemistry*, edited by S. Wilsom (Wiley, Chichester, 2003), Vol. 3, pp. 356–369.
[4]T. P. Snow and B. J. McCall, Annu. Rev. Astron. Astrophys. **44**, 367 (2006).
[5]T. Oka, in *Dissociative Recombination of Molecular Ions with Electrons*, edited by S. L. Guberman (Springer US, 2003), pp. 209–220.
[6]M. Larsson and A. E. Orel, *Dissociative Recombination of Molecular Ions* (Cambridge University Press, 2008).
[7]R. Johnsen and S. L. Guberman, in *Advances in Atomic, Molecular, and Optical Physics*, edited by P. B. E. Arimondo and C. Lin (Academic Press, 2010), Vol. 59, pp. 75–128.
[8]T. Albertsson, N. Indriolo, H. Kreckel, D. Semenov, K. N. Crabtree, and T. Henning, Astrophys. J. **787**, 44 (2014).
[9]H. Kreckel, M. Motsch, J. Mikosch, J. Glosík, R. Plašil, S. Altevogt, V. Andrianarijaona, H. Buhr, J. Hoffmann, L. Lammich, M. Lestinsky, I. Nevo, S. Novotny, D. A. Orlov, H. B. Pedersen, F. Sprenger, A. S. Terekhov, J. Toker, R. Wester, D. Gerlich, D. Schwalm, A. Wolf, and D. Zajfman, Phys. Rev. Lett. **95**, 263201 (2005).
[10]B. J. McCall, A. J. Huneycutt, R. J. Saykally, T. R. Geballe, N. Djuric, G. H. Dunn, J. Semaniak, O. Novotny, A. Al-Khalili, A. Ehlerding, F. Hellberg, S. Kalhori, A. Neau, R. Thomas, F. Osterdahl, and M. Larsson, Nature **422**, 500 (2003).
[11]A. Wolf, H. Kreckel, L. Lammich, D. Strasser, J. Mikosch, J. Glosík, R. Plašil, S. Altevogt, V. Andrianarijaona, H. Buhr, J. Hoffmann, M. Lestinsky, I. Nevo, S. Novotny, D. Orlov, H. Pedersen, A. Terekhov, J. Toker, R. Wester, D. Gerlich, D. Schwalm, and D. Zajfman, Philos. Trans. R. Soc., A **364**, 2981 (2006).
[12]A. Petrignani, H. Kreckel, M. H. Berg, S. Altevogt, D. Bing, H. Buhr, M. Froese, M. Grieser, J. Hoffmann, B. Jordon-Thaden, C. Krantz, M. B. Mendes, O. Novotný, S. Novotny, D. A. Orlov, S. Reinhardt, and A. Wolf, J. Phys.: Conf. Ser. **192**, 012022 (2009).
[13]B. A. Tom, V. Zhaunerchyk, M. B. Wiczer, A. A. Mills, K. N. Crabtree, M. Kaminska, W. D. Geppert, M. Hamberg, M. af Ugglas, E. Vigren, W. J. van der Zande, M. Larsson, R. D. Thomas, and B. J. McCall, J. Chem. Phys. **130**, 031101 (2009).
[14]H. Kreckel, O. Novotný, K. N. Crabtree, H. Buhr, A. Petrignani, B. A. Tom, R. D. Thomas, M. H. Berg, D. Bing, M. Grieser, C. Krantz, M. Lestinsky, M. B. Mendes, C. Nordhorn, R. Repnow, J. Stützel, A. Wolf, and B. J. McCall, Phys. Rev. A **82**, 042715 (2010).
[15]A. Petrignani, S. Altevogt, M. H. Berg, D. Bing, M. Grieser, J. Hoffmann, B. Jordon-Thaden, C. Krantz, M. B. Mendes, O. Novotný, S. Novotny, D. A. Orlov, R. Repnow, T. Sorg, J. Stützel, A. Wolf, H. Buhr, H. Kreckel, V. Kokoouline, and C. H. Greene, Phys. Rev. A **83**, 032711 (2011).
[16]B. J. McCall, A. J. Huneycutt, R. J. Saykally, N. Djuric, G. H. Dunn, J. Semaniak, O. Novotný, A. Al-Khalili, A. Ehlerding, F. Hellberg, S. Kalhori, A. Neau, R. D. Thomas, A. Paal, F. Österdahl, and M. Larsson, Phys. Rev. A **70**, 052716 (2004).
[17]M. Larsson, Philos. Trans. R. Soc., A **370**, 5118 (2012).
[18]H. Kreckel, A. Petrignani, O. Novotný, K. Crabtree, H. Buhr, B. J. McCall, and A. Wolf, Philos. Trans. R. Soc., A **370**, 5088 (2012).
[19]P. Dohnal, M. Hejduk, J. Varju, P. Rubovič, Š. Roučka, T. Kotrík, R. Plašil, J. Glosík, and R. Johnsen, J. Chem. Phys. **136**, 244304 (2012).
[20]P. Dohnal, M. Hejduk, J. Varju, P. Rubovič, Š. Roučka, T. Kotrík, R. Plašil, R. Johnsen, and J. Glosík, Philos. Trans. R. Soc., A **370**, 5101 (2012).
[21]J. Varju, M. Hejduk, P. Dohnal, M. Jílek, T. Kotrík, R. Plašil, D. Gerlich, and J. Glosík, Phys. Rev. Lett. **106**, 203201 (2011).
[22]M. Hejduk, P. Dohnal, J. Varju, P. Rubovič, R. Plašil, and J. Glosík, Plasma Sources Sci. Technol. **21**, 024002 (2012).
[23]R. Plašil, J. Glosík, V. Poterya, P. Kudrna, J. Rusz, M. Tichý, and A. Pysanenko, Int. J. Mass Spectrom. **218**, 105 (2002).
[24]I. Korolov, R. Plašil, T. Kotrík, P. Dohnal, and J. Glosík, Int. J. Mass Spectrom. **280**, 144 (2009).
[25]P. Macko, G. Bánó, P. Hlavenka, R. Plašil, V. Poterya, A. Pysanenko, O. Votava, R. Johnsen, and J. Glosík, Int. J. Mass Spectrom. **233**, 299 (2004).
[26]J. Glosík, I. Korolov, R. Plašil, O. Novotný, T. Kotrík, P. Hlavenka, J. Varju, I. A. Mikhailov, V. Kokoouline, and C. H. Greene, J. Phys. B: At. Mol. Opt. **41**, 191001 (2008).
[27]P. Dohnal, P. Rubovič, T. Kotrík, M. Hejduk, R. Plašil, R. Johnsen, and J. Glosík, Phys. Rev. A **87**, 052716 (2013).
[28]T. Kotrík, P. Dohnal, Š. Roučka, P. Jusko, R. Plašil, J. Glosík, and R. Johnsen, Phys. Rev. A **83**, 032720 (2011).
[29]T. Kotrík, P. Dohnal, P. Rubovič, R. Plašil, Š. Roučka, S. Opanasiuk, and J. Glosík, Eur. Phys. J. Appl. Phys. **56**, 24011 (2011).
[30]R. Johnsen, P. Rubovič, P. Dohnal, M. Hejduk, R. Plašil, and J. Glosík, J. Phys. Chem. A **117**, 9477 (2013).
[31]P. Dohnal, P. Rubovič, Á. Kálosi, M. Hejduk, R. Plašil, R. Johnsen, and J. Glosík, Phys. Rev. A **90**, 042708 (2014).
[32]J. Glosík, R. Plašil, I. Korolov, T. Kotrík, O. Novotný, P. Hlavenka, P. Dohnal, J. Varju, V. Kokoouline, and C. H. Greene, Phys. Rev. A **79**, 052707 (2009).
[33]S. Fonseca dos Santos, V. Kokoouline, and C. H. Greene, J. Chem. Phys. **127**, 124309 (2007).
[34]C. Jungen and S. T. Pratt, Phys. Rev. Lett. **102**, 023201 (2009).
[35]L. Pagani, C. Vastel, E. Hugo, V. Kokoouline, C. H. Greene, A. Bacmann, E. Bayet, C. Ceccarelli, R. Peng, and S. Schlemmer, Astron. Astrophys. **494**, 623 (2009).
[36]K. N. Crabtree and B. J. McCall, Philos. Trans. R. Soc., A **370**, 5055 (2012).
[37]K. N. Crabtree, N. Indriolo, H. Kreckel, B. A. Tom, and B. J. McCall, Astrophys. J. **729**, 15 (2011).
[38]N. Indriolo and B. J. McCall, Astrophys. J. **745**, 91 (2012).
[39]J. Glosík, G. Bánó, R. Plašil, A. Luca, and P. Zakouřil, Int. J. Mass Spectrom. **189**, 103 (1999).
[40]M. R. Mahdavi, J. B. Hasted, and M. M. Nakshbandi, J. Phys. B: At. Mol. Opt. **4**, 1726 (1971).
[41]P. Rubovič, P. Dohnal, M. Hejduk, R. Plašil, and J. Glosík, J. Phys. Chem. A **117**, 9626 (2013).
[42]I. Korolov, R. Plašil, T. Kotrík, P. Dohnal, O. Novotný, and J. Glosík, Contrib. Plasma Phys. **48**, 461 (2008).
[43]J. Glosík, R. Plašil, T. Kotrík, P. Dohnal, J. Varju, M. Hejduk, I. Korolov, Š. Roučka, and V. Kokoouline, Mol. Phys. **108**, 2253 (2010).
[44]E. Alge, N. G. Adams, and D. Smith, J. Phys. B: At. Mol. Opt. **16**, 1433 (1983).
[45]E. Ilisca, Prog. Surf. Sci. **41**, 217 (1992).
[46]S. Yucel, Phys. Rev. B **39**, 3104 (1989).
[47]I. Zymak, M. Hejduk, D. Mulin, R. Plašil, J. Glosík, and D. Gerlich, Astrophys. J. **768**, 86 (2013).
[48]M. Cordonnier, D. Uy, R. M. Dickson, K. E. Kerr, Y. Zhang, and T. Oka, J. Chem. Phys. **113**, 3181 (2000).
[49]F. Grussie, M. H. Berg, K. N. Crabtree, S. Gärtner, B. J. McCall, S. Schlemmer, A. Wolf, and H. Kreckel, Astrophys. J. **759**, 21 (2012).

[50]J. Glosík, M. Hejduk, P. Dohnal, P. Rubovič, Á. Kálosi, and R. Plašil, EPJ Web Conf. **84**, 01002 (2015).
[51]C. M. Lindsay and B. J. McCall, J. Mol. Spectrosc. **210**, 60 (2001).
[52]P. Dohnal, M. Hejduk, P. Rubovič, J. Varju, Š. Roučka, R. Plašil, and J. Glosík, J. Chem. Phys. **137**, 194320 (2012).
[53]E. A. Mason and E. W. McDaniel, *Transport Properties of Ions in Gases* (Wiley, New York, 1988).
[54]J. Stevefelt, J. Boulmer, and J. F. Delpech, Phys. Rev. A **12**, 1246 (1975).
[55]W. Lindinger and D. L. Albritton, J. Chem. Phys. **62**, 3517 (1975).
[56]V. Wakelam, E. Herbst, J.-C. Loison, I. W. M. Smith, V. Chandrasekaran, B. Pavone, N. G. Adams, M.-C. Bacchus-Montabonel, A. Bergeat, K. Béroff, V. M. Bierbaum, M. Chabot, A. Dalgarno, E. F. van Dishoeck, A. Faure, W. D. Geppert, D. Gerlich, D. Galli, E. Hébrard, F. Hersant, K. M. Hickson, P. Honvault, S. J. Klippenstein, S. L. Picard, G. Nyman, P. Pernot, S. Schlemmer, F. Selsis, I. R. Sims, D. Talbi, J. Tennyson, J. Troe, R. Wester, and L. Wiesenfeld, Astrophys. J., Suppl. Ser. **199**, 21 (2012).